Modeling Genome-wide by Environment Interactions through Omnigenic Interactome Networks

Haojie Wang[1,#], Meixia Ye[1,#], Yaru Fu[1], Xuli Zhu[1], Wenhao Bo[1], Ang Dong[1], Libo Jiang[1], Christopher Griffin[2], Rongling Wu[1,3,4,*]

[1]Beijing Advanced Innovation Center for Tree Breeding by Molecular Design, College of Biological Sciences and Technology, Beijing Forestry University, Beijing 100083, China
[2]Applied Research Laboratory, The Pennsylvania State University, University Park, PA 16802, USA
[3]Center for Statistical Genetics, Departments of Public Health Sciences and Statistics, The Pennsylvania State University, Hershey, PA 17033, USA

[#]These authors contributed to this work equally.
[4]Lead Contact
[*]Corresponding author: Rongling Wu, rwu@phs.psu.edu

Keywords: gene-environment interaction, epistasis, genetic network, omnigenic model, variable selection, developmental modularity

Highlights

- Complex traits are controlled by all genes carried by the organism and its surrounding environment
- Existing linear models built on single genes fail to dissect the complexity of genome-wide genotype-environment (G-E) interplay
- We propose a computational model for reconstructing multilayer omnigenic networks driving G-E interactions
- The model allows us to retrieve the causality of epistasis and integrate bidirected epistasis into the mechanistic landscape of G-E interactions
- Our multiplayer networks facilitate the incorporation of genome-wide G-E interactions into genome-wide association studies

Abstract

How genes interact with the environment to shape phenotypic variation and evolution is a fundamental question intriguing to biologists from various fields. Existing linear models built on single genes are inadequate to reveal the complexity of genotype-environment (G-E) interactions. Here, we develop a conceptual model for mechanistically dissecting G-E interplay by integrating previously disconnected theories and methods. Under this integration, evolutionary game theory, developmental modularity theory, and a variable selection method allow us to reconstruct environment-induced, maximally informative, sparse, and casual multilayer genetic networks. We design and conduct two mapping experiments using a desert-adapted tree species to validate the biological application of the new model. The model identifies

previously uncharacterized molecular mechanisms that mediate trees' response to saline stress. Our model provides a tool to comprehend the genetic architecture of trait variation and evolution and trace the information flow of each gene toward phenotypes within omnigenic networks.

Keywords: genetic architecture, epistasis, complex trait, growth, genetic network, statistical model

Introduction

Complex traits of an organism are jointly controlled by its genes and the environment where it lives. The impact of G-E interactions, i.e., differential expression of genetic effects between environments, involves a complex but not yet fully understood mechanism (Hunter 2005; Sparrow et al. 2012; El-Soda et al. 2014; McAllister et al. 2017; Esposito et al. 2018; Li et al. 2019; Boyce et al. 2020). In classic quantitative genetic studies, a linear additive model is used to partition total phenotypic variance into its genetic, environment, and G-E interaction components at one or two genes at a time (El-Soda et al. 2014; Li et al. 2019; Boyce et al. 2020). This approach has been instrumental for identifying key genes that interact with the environment (Wu 1998; Wang et al. 2019; Sulc et al. 2020; Diouf et al. 2020), but it fails to reveal how genes change their effects, as a cohesive whole, in response to environmental cues. With the availability of full genome sequences, genome-wide by environment interaction studies (GWEIS) have brought G–E interaction analyses into the context of genome-wide association studies (GWAS), undoubtedly expected to become a routine approach for mapping complex traits (Thomas 2010; Aschard 2016; McAllister et al. 2017; Arnau-Soler et al. 2019; Boyce et al. 2020). A new theory, known as omnigenic theory, has emerged to recognize that complex traits or diseases are governed by all genes through network behavior carried by the organism (Boyle et al. 2017; Liu et al. 2019). Although it is clear that such networks are well orchestrated and high-dimensional, we know little about their structure and organization, how they can be incorporated into GWEIS, and how they play a role in shaping the organism's environmental adaptation through mediating G-E interplay.

To address the above issues, the first step is to reconstruct informative, omnigenic genetic networks encapsulated by all gene-gene interactions that biologically exist and act throughout the whole genome. There are several major challenges to achieve this step. First, reconstructing an omnigenic network from all genome-wide genes is not only computationally prohibited, but also biologically unjustified given that the occurrence of all possible pairwise links among biological entities in a cell may impair the cell's robustness against perturbations (May 1972; Gross et al. 2009; Allesina and Tang 2012; Busiello et al. 2017). Second, unlike gene expression data that are collected on individual samples, the genetic effect of a locus on a complex trait represents an overall behavior of all samples and, thus, do not conform to the data structure of network inference (Vijesh et al. 2013; Wang and Huang 2014; Han et al. 2016; Mulligan et al. 2017). Third, in quantitative genetics, genetic interactions between different loci, called epistasis, are not directed (Bateson 1907; Sackton and Hartl 2016; Costanzo et al. 2019), but the causality and the sign of causality are of critical importance to understanding the mechanisms of epistasis and implementing it into practical gene editing schemes.

Here, we develop a computational model for identifying large-scale genetic networks from genetic linkage or association mapping data and interrogating how these networks topologically change as a result of the environment to mediate G-E interactions. This model integrates functional mapping, a dynamic model for mapping complex traits (Ma et al. 2002; Wu et al. 2004; Wu and Lin 2006; Li and Sillanpaa 2015; Lyra et al. 2020), functional clustering (Kim et al. 2008; Wang et al. 2012), and evolutionary game theory (Smith and Price 1973; Axelrod and Hamilton 1981; McNamara 2013) into a unified framework. Under this framework, a system of nonlinear Lotka-Volterra (nLV) ordinary differential equations (ODEs) is derived as quantitative descriptors of epistasis and networks. We show that the new model can better dissect the genetic contribution of each gene to G-E interactions through its direct and indirect roadmaps. To validate the utility of the model, we design and conduct two independent but complementary ecological mapping experiments using an intraspecific full-sib family and a panel of wild germplasm from Euphrates poplar (*Populus euphratica* Oliver), an only tree that can survive, grow, and reproduce in the desert (Soleimani et al. 2014; Zhang et al. 2020). We characterize previously unknown genetic interactions that mediate the tree's resistance to saline stress through G-E interactions.

Results

Temporal pattern of genetic effects revealed by functional mapping

The first ecological mapping experiment includes 106 full-sib hybrids of *P. euphratica*, cultured in salt-free (control) and salt-exposed (stress) media (Fig. S1), using clonal replicates. The growth of adventitious roots can be fitted by a modified logistic growth equation including a three-parameter logistic equation subtracted by an exponential equation to adjust for the asymptote-unknown growth curve (Fig. 1**A**). As expected, roots generally grow better in the control than stress condition ($P < 0.05$), but the path to reach maximal growth differs between two treatments. Roots display a slightly lower rate of growth, take a longer time to reach the maximum growth rate (t_I: 25.9 vs. 20.7), and a longer linear growth length (Δ: 34.6 vs. 27.9), collectively expected to produce greater asymptotic growth (a: 24.5 vs. 13.4) in the control than stress condition (Fig. 1**A**). However, treatment-induced differences in root growth curve vary among offspring genotypes, with some genotypes having no differences and others having notable differences. Although most genotypes perform better in the control than stress condition, a portion of genotypes (21.7%) exhibit an inverse pattern of differences. Taken together, remarkable G-E interactions are detected to affect the growth trajectory of adventitious roots in the linkage mapping experiment.

We implement a bivariate functional mapping (biFunMap) model to map significant loci (called QTLs) that affect the total length of adventitious roots for *P. euphratica* at least under one condition (Fig. 1**B**). The advantage of biFunMap is to elucidate the developmental pattern of the genetic effect exerted by a QTL (Fig. 1**C**). Of a total of 33 QTLs detected, some, such as Q1424, Q1853, Q1871, etc., are "pleiotropic" QTLs responsible for root growth expressed in both environments, whereas others only affect root growth in one environment; for example, Q2245 and Q3568 are control-specific QTLs whereas Q4040 and Q5606 are stress-specific QTLs. The temporal pattern of how QTLs affects root growth varies among loci; some QTLs, such as Q35 and Q1424, consistently increase their genetic effects over time, whereas others exhibit time-decreasing effects (e.g., Q1275) or periodically varying effects (e.g., Q5770). Most QTLs detected were annotated by GO analysis to candidate genes that mostly mediate tree-typical

molecular and biological processes (Table S1). Although this consistency shows the biological relevance of functional mapping as a statistical approach of QTL mapping, we argue that this reductionist-based approach may have missed many loci that are not necessarily significant by themselves but negatively regulated by other loci. To retrieve these missing genetic effects, we need to partition the net genetic effect of a locus detected by functional mapping into its independent effect (due to the intrinsic capacity of this locus) and dependent effect (resulting from the influence of other loci). As the first step of this partition, we used biFunMap to estimate the genetic effect curve of each SNP on adventitious root growth in control and stress conditions (see the Star*Methods).

Network communities detected by the temporal pattern of genetic effects

Developmental modularity theory suggests that development occurs through a series of discrete and interacting modules (Riedl 1978; Gilbert et al. 1996; Raff 1996; Wagner 1996) within which entities are more strongly connected to each other than to those from other modules. This theory provides a basis for clustering a whole pool of genome-wide SNPs into distinct modules based on the similarity of genetic effect curves. We implemented bivariate functional clustering (biFunClu) to classify 8,305 SNPs expressed in control and stress conditions into different modules. The optimal number of modules is found to be 400 on parsimony, suggesting that an 8,305-node genetic network for root growth can be broken down into 400 distinct network communities. The genetic effect of each module displays a specific temporal pattern across control and stress conditions. We illustrate nine representative modules M1 – M9 (Fig. 2**A**), among which pronounced discrepancies exist in the temporal pattern of genetic effects under both conditions. Some modules have a similar pattern between the two treatments, but many others are treatment-specific. Some modules have larger genetic effects in the control than stress condition, but others exhibit an inverse pattern. All these differences in the time-dependent change of genetic effects contribute to the complexity of the genetic architecture of root growth in response to environmental cues.

Multilayer networks

We calculated the mean genetic effect curves of each module and used them to reconstruct inter-community genetic networks under control and stress conditions (Fig. 2**B**). Such networks are

called *macroscopic genetic networks* given that their nodes represent a collective effect of all SNPs within a module. Macroscopic networks under both control and stress conditions are highly sparse, with module-module links that only occur among 2.07 – 2.20% of full pairwise links. Directional positive epistasis and directional negative epistasis together predominate the links, but relative to the former, the latter is richer by 34.7% in the stress condition and slightly less rich in the control condition, suggesting that genes tend to be antagonistic in the stressful environment. Reciprocal positive epistasis and reciprocal negative epistasis together occupy a small portion of links in each network (1.88 – 2.1%). For a module, a link is said to be outgoing if this module activates or inhibits other modules, or incoming if it is activated or inhibited by other modules. Outgoing and incoming links reflect different roles of a module played in network structure and behavior. We plotted the distribution of outgoing links and incoming links across individual modules (middle panel; Fig. 2**B**). Although outgoing links and incoming links are similar in number, their allocations to modules are dramatically different. Outgoing links are predominated by a small number of modules, whereas incoming links are distributed relatively uniformly over modules, suggesting that a few "leaders" modulate the majority of "subordinates" in the genetic networks. We found that the distribution of both outgoing and incoming links differs dramatically between the control and stress networks. In particular, the modules that serve as a leader in one network become subordinates in the other network.

Thirty-three QTLs detected by biFunMap (Fig. 1**B**) reside within 30 different modules (i.e., communities), suggesting that these QTLs basically play a unique role in governing root growth. Most QTL-containing modules are located at or near the periphery of the networks, with the number of incoming links they receive being larger than the number of outgoing links they exert (Fig. 2**B**). We reconstructed genetic networks at the SNP level for each QTL-containing module. We call such SNP-SNP networks *microscopic genetic networks*. Modules M177 and M178 are only two modules containing more than one QTLs. These two modules have 16 and 22 SNPs, respectively, whose microscopic networks were reconstructed and compared between control and stress conditions (Fig. 3). In all cases, only a small portion of SNPs dominate outgoing links, whereas all SNPs receive incoming links. However, the distribution of both types of links, especially outgoing links, is very different between two conditions. Taken together, it suggests that microscopic networks follow a general rule under stress-free and stress-exposed conditions,

but the organization of SNPs used to execute this rule is largely environment-dependent, implicating strong G-E interactions. Under control and stress conditions, we found that QTLs basically serve as regulatees activated or inhibited by other SNPs. For example, in the microscopic network of M177, QTL1853 receives directional positive epistasis from four SNPs (1870, 3235, 5747, and 7094) and two SNPs (5748 and 6047) under the control and stress conditions, respectively, but it exerts no outgoing links under each condition (Fig. 3**A**). A similar finding is true for the microscopic network of M178 (Fig. 3**B**).

Module M22 is the largest QTL-containing module containing 66 SNPs. We used biFunClu to further divide this module into eight submodules (coded as SM1_22, …, SM8_22). In the so-called *mesoscopic genetic networks* reconstructed from these submodules (Fig. 4**A**), QTL-containing submodule SM6_22 activates other submodules in the stress-free network but is inhibited by other submodules in the stress network. There is a loop of activation SM6_22 → SM2_22 → SM8_22 → SM7_22 → SM5_22 → SM4_22 → SM2_22 in the stress-free network, but this loop does not exist in the stress network. The microscopic network of SM6_22 exhibits a considerable difference in network organization between control and stress conditions, as revealed by the environment-dependent distribution of outgoing and incoming links (Fig. 4**B**).

Causal dissection of epistatic networks

Microscopic networks at the individual SNP level provide a roadmap to unveil a detailed causal discrepancy of epistasis between control and stress conditions. We dissected how the influence of a QTL is determined by other insignificant SNPs in each QTL-containing microscopic network. We found that the same QTLs perform differently between stress-free and stress-exposed conditions. In general, when a QTL is expressed under the control condition, it is more likely to be affected by other SNPs, and to a larger extent, than when it is expressed under the stress condition. Thus, under the control condition, the net genetic effect of a QTL is dramatically different from its independent effect resulting from its intrinsic capacity, whereas the net genetic effect of a QTL is more similar to its independent effect under the stress condition. For example, two QTLs Q1853 and Q4514, included in the microscopic network of module M177, were found to affect root growth under both control and stress conditions by biFunMap (Fig. 5**A**). Q1853 located on chromosome 2 is found to reside in the *HIGH-LEVEL*

EXPRESSION OF SUGAR-INDUCIBLE GENE2-LIKE1 (*HSL1*) gene regulating plant chromatin conformation. Under the salt-free condition, the expression of *HSL1* is promoted by four SNPs in a cyclically positive and negative pattern, of which SNP S1870 is the Cys_2/His_2-type zinc finger transcription factor, *ZAT12*. SNP S5747 is an F-box protein-encoding gene *SKIP23*, and S3235 and S7094 have uncharacterized functions (Fig. S2). Because of up-regulations by these SNPs, the net genetic effect of QTL Q1853 is larger than its independent effect under the control condition. When exposed to salt stress, *HSL1* is slightly promoted by S5748 (probable ubiquitin-conjugating enzyme *E2SKP1*-like protein 1B gene) and S6829 (protein *IQ-DOMAIN 14*-like gene) (Fig. 5**A**, Fig. S2). Q4514 on chromosome 8 is up-regulated by S6829 and, meanwhile, to a similar extent, down-regulated by S1870 under the salt-free condition (Fig. 5**A**). We found that S1870 promotes Q1853 but inhibits Q4514 in the salt-free condition, whereas S6829 promotes Q4514 under both salt-free and salt-exposed conditions (Fig. S2). In contrast to the control case, Q1853 and Q4514 are slightly affected by other SNPs under the stress condition.

The microscopic network reconstructed from module M178 contains three QTLs, each of which affects adventitious root growth in a different way depending on whether the environment is stress-free or stress-exposed (Fig. 5**B**). Under the control condition, all QTLs perform better than expected from their intrinsic capacity because they receive overall positive up-regulation from other SNPs. Yet, none of them is largely affected by other SNPs under the stress condition so that their net genetic effects are similar to their independent effects. A similar environment-dependent pattern of genetic effects was found for Q1275 located within a submodule of module M22 (Fig. 5**C**). Figure S2 illustrates results about gene enrichment analyses of all QTLs and the SNPs that regulate the QTLs.

Regulatory role of insignificant loci

Traditional approaches can only detect the significance of QTLs in terms of their net genetic effects. It is possible that those insignificant SNPs based on statistical testing would have strong independent effects (in isolation), but are canceled unfortunately by negative epistatic effects through incoming links. Our proposed model can address this previously neglected issue. From the biFunMap Manhattan plot (Fig. 1**B**), we randomly chose several insignificant SNPs (with low LRs at the bottom) to reconstruct microscopic genetic networks involving these SNPs.

Two insignificant SNPs, S2010 on chromosome 3 and S6422 on chromosome 13, are located in the microscopic network of module 114 (Fig. 6**A**). S2010 is annotated to gene *POP033-J16*, which is not only positively up-regulated but also negatively down-regulated by other SNPs (regulators) in each environment. The negative regulators include function-known genes, i.e., *MYB308* (SNP4510), *At1g67480* (SNP6376), and *BRL1* (SNP7778) in the salt-free condition and *RBK2* (SNP2882), *RP23-231B13* (SNP3879), and *Phototropin-2 ATP binding* (SNP5726) in the salt-exposed condition (Fig. S3). Collectively, S2010 receives much larger down-regulation than up-regulation, making it fail to display its actually remarkable independent effects (Fig. 6**A**). Similarly, S6422, annotated to gene *SEC6*, is regulated by many other SNPs, many of which reside in candidate genes (Fig. S3). Yet, collectively, this SNP is down-regulated, to a larger extent, than up-regulated, which cancels its independent effect. As can be seen from the above two examples, insignificant SNPs may possibly exert their pronounced genetic impacts on root growth if their negative regulators are silenced.

Similar phenomena are also found for insignificant S1235 on chromosome 2 and S2970 on chromosome 5 involved in the microscopic network of module M364 (Fig. 6**B**), whose independent effects are counteracted by directional negative epistasis through incoming links. Taken together, SNPs detected to be insignificant based on traditional testing of marginal effects may not actually be insignificant because their independent effects may be canceled by down-regulation from negative regulators. The type of regulators that regulate a particular SNP, as well as the sign and strength of such regulation, may vary over environment, likely acting as an important driver of G-E interactions.

Model validation by a GWAS experiment

By building and using a GWAS population of *P. euphratica*, we designed an additional ecological mapping experiment laid out under salt-free and salt-exposed treatments with clonal replicates. This population includes nearly one quarter of million SNPs, a number 29 times as large as that used in the first experiment. Reconstructing genetic networks from such a high-dimensional data can better demonstrate the unique power of our model to handle complex biological issues. As expected, clonal seedlings of *P. euphratica* grow taller stems in control than

stress treatments, and trees under these conditions are characterized by different heterochronic features (Fig. S4A). BiFunMap detects a total of 52 QTLs from 241,990 SNPs genotyped throughout the *Populus* genome (Fig. S4B), whose genetic effects on stem height growth exhibit different temporal patterns under two conditions (Fig. S4C).

Using a BIC analysis, biFunClu identifies 99 modules, each with a different temporal pattern of genetic effects in two conditions, among all SNPs (Fig. S5). In the other word, a 241,990-node large network contains 99 well-delimited network communities. The 52 QTLs detected are dispersed in 29 communities, of which 28 contain 1-2 QTLs and the remaining one contains 3 QTLs, suggesting that the pattern of time-varying genetic effects is quite QTL-specific. We reconstruct a 99-node macroscopic network at the top level (layer 1) under both control and stress conditions (Fig. S6). We further break down those big communities into subcommunities that form mesoscopic networks at layer 2 and then reconstruct SNP-SNP networks for each subcommunity at the bottom level (layer 3) (Fig. S6). From such a multilayer genetic network, we can characterize how each SNP (including QTLs) affects stem height growth and test how it interacts with the environment through its independent (main) and dependent (epistatic) effects.

Figure S7 illustrates examples of QTL-environment interactions for stem height growth through epistatic effects from submodule SMx_x of module Mx. QTL Q90199 has a similar independent genetic effect under two treatments, but it is observed to have a larger genetic effect in control than in stress condition because it receives larger down-regulation from other loci in the former but larger up-regulation in the latter. Likewise, QTL Q186458 exerts a treatment-invariant independent effect on stem height growth, but because of the large favorable up-regulation it receives in saline stress, this QTL has a much larger observed genetic effect in this condition than in control (Fig. S7). There are many other examples that show the different roles of individual QTLs in mediating G-E interactions. According to the temporal pattern of net genetic effect in control and stress conditions, QTLs Q90199, Q190340, and Q186458 are sorted into the same module M58 that forms a network community (Fig. S8A), but they perform differently in many ways (Fig. S8B). These QTLs each have a larger independent effect in control than in stress, but they are observed to have no treatment-dependent difference in net genetic effect, because they receive negative regulation in control but positive regulation in stress. It is

interesting to see that QTLs Q90199 and Q190340 each receive both large positive regulation and large negative regulation from different loci in control but only slight regulation from the same loci in stress. We elucidate and dissect the effect curves of all other QTLs in Fig. S9. Taken together, G-E interactions may not only be caused by environment-induced main net genetic effects, but also, to a large extent, by environment-induced independent genetic effects and dependent genetic effects. While existing models can only characterize the first cause, our model can better depict the genetic landscape of G-E interactions by encapsulating all these causes into multilayer networks.

In addition to the dissection of QTL effects, we also partition the net genetic effects of all insignificant SNPs into their independent and dependent effect components under control and stress conditions. This allows us to identify the reasons why they are not significant. Figure S10 illustrates examples in which three SNPs each have a subtle net genetic effect, but with large independent genetic effects. The independent effects of these SNPs cannot be expressed because of negative down-regulation by other loci. Thus, by knocking off those negative regulators, their independent genetic effects can fully act to affect stem height growth in specific environments. If an insignificant SNP receives both positive up-regulation and negative down-regulation, its genetic effect on stem height can be augmented by adding positive dependent effects to its independent effect when negative regulators are silenced. It can be seen that we can potentially recover a portion of the missing heritability if the roadmap of how each SNP affects a given trait is traced via our multilayer interactome networks. Together, results from genome-wide linkage mapping and association mapping have consistently validated the biological relevance and novelty of our new model.

Discussion

Almost all complex traits involve genetic and environmental components and their multileveled intertwined interactions. A number of genetic mapping and association studies have identified thousands of common loci associated with complex traits or diseases (Tam et al. 2019), but the pattern of how the interplay of these loci with the environment mediates phenotypic variation remains unclear. There are several reasons that make it difficult to study G-E interactions. First,

relative to studies targeting either genetic or main environmental effects alone, G-E interaction studies require much larger sample sizes (which may be difficult to meet in many studies) to reach any reasonable conclusion (Aschard 2016; McAllister et al. 2017). Further, when a study is performed on a genome-wide scale, even larger sample sizes are required to account for multiple comparisons (Thomas 2010: Murcray et al. 2011). Second, the methodology of most G-E interaction studies is based on reductionist thinking, aimed to detect key individual loci that display interactions with the environment (Wu 1998; El-Soda et al. 2014; Boyce et al. 2020), but the genetic architecture of complex traits is likely to be omnigenic; i.e., trait control involves all genes an organism may carry on its genome (Boyle et al. 2017; Liu et al. 2019). Third, perhaps, and most importantly, these analytical models are derived from linear regression, but indeed it is likely that G-E interactions operate in a complex nonlinear fashion (del Sol et al. 2010; Wu and Cui 2013; Wu et al. 2018). Nonlinearities between genes and environment resulting from substantial uncertainties and random effects across timescales (Gottlieb 2007) can help trait phenotypes to maintain their robustness to perturbations in environmental exposures (Félix and Barkoulas 2015). While many studies have embedded epistatic interactions into genome-wide mapping (Sackton and Hartl 2016; Costanzo et al. 2019), the incorporation of G-E interactions has increasingly become an essential next consideration of genetic mapping and association studies (Thomas 2010; Aschard 2016; McAllister et al. 2017; Arnau-Soler et al. 2019; Boyce et al. 2020). Unfortunately, there is still little methodology to characterize the role of genome-wide G-E interactions, especially genome-wide epistasis by environmental interaction, in contributing to phenotypic variation and evolution.

In this article, we present a computational model for integrating G-E interactions into the GWEIS context through omnigenic networks. This approach presents a paradigm shift from linear, reductionist thinking to a nonlinear, holistic philosophy, which is less reliant on sample size. All these merits stem from the seamless integration of functional mapping, evolutionary game theory, and developmental modularity theory, implemented with the state-of-art of high-dimensional statistical theory and methods. Functional mapping integrates the mathematical aspect of trait development to estimate the net genetic effect of each SNP that changes over time in a certain pattern, whereas evolutionary game theory allows us to decompose the net effect into its independent and dependent components through nLV equations. Originating in economic

theory, game theory asserts that a rational player tends to maximize its payoff by choosing an optimal strategy based on the strategies of other players (von Neumann and Morgenstern 1943; Nash 1950). Evolutionary game theory extends this theory by relaxing the rationality assumption (Smith and Price 1973). By estimating the independent and dependent effects of a genetic locus, our model can estimate and test how this locus affects trait development directly through its own capacity (main effects) and indirectly through the regulation of other loci (epistatic effects). While traditional quantitative genetic methods can only estimate the magnitude and sign of epistasis (Sackton and Hartl 2016), our model can further characterize the causality of epistasis, the direction of the causality, and the reciprocity of the causality. Because of its capacity in effect decomposition, the model can shed light on the mechanistic details of genetic control by tracing the roadmap of how each gene affects a trait. For example, QTL Q1853 (in module M177) has a larger effect on the adventitious root growth of *P. euphratica* in salt-free than salt-exposed conditions, although it is significant in both environments by biFunMap (Fig. 5**A**). Yet, its large effect in the control condition is virtually contributed by the directional positive epistasis this QTL receives from regulatory SNPs S1870, S3235, S5747, and S7094 rather than due to its own capacity. In contrast, SNPs S2970 and S1235 are insignificant in terms of their net genetic effect, but both of them intrinsically have a large independent effect, which is counteracted by regulatory SNPs (Fig. 6**C**). These two examples show the critical importance of defining causal epistasis for the precise genetic dissection and editing of complex traits.

The networks reconstructed from our model can be omnigenic, which include a complete pool of genome-wide SNPs. Such large-scale networks can be inferred by integrating modularity theory and sparsity theory into our model framework. Both theories suggest that not all pairwise links among genes function for complex systems in order to buffer against stochastic perturbations (May 1972; Gross et al. 2009; Allesina and Tang 2012; Busiello et al. 2017), leading to patched, sparse networks. Functional clustering is implemented to break down a whole network into its distinct network communities in which genes are linked more strongly to each other than to those from other communities. Variable selection is incorporated to select a small set of the most significant links for a given gene. The simultaneous implementation of these two approaches allows multilayer sparse networks to be reconstructed. At the top layer, the network reflects the interconnections of network communities, called macroscopic networks, whereas those at the

lower-level layers characterize more fine-grained structures composed of subcommunity networks all the way down to SNP-SNP interaction networks (i.e., microscopic networks). Microscopic networks are the target networks in which epistasis, its direction, sign, magnitude, and roadmap, can be precisely mapped and edited in genomic practices. Macroscopic networks, and mesoscopic networks, i.e., networks reconstructed from submodules, are considered as genetic contexts to manipulate microscopic networks.

In analyzing two mapping experiments of *P. euphratica*, we show that multilayer networks of bidirectional, signed, and weighted interactions can be used to dissect G-E interactions. We found that the genetic architecture of root growth (below ground) and stem growth (above ground) changes in response to salt stress not only through differentiated expression of single QTLs but also, more precisely, through the interaction networks of genome-wide SNPs. For example, almost all QTLs detected by functional mapping are, to a larger extent, regulated by many more SNPs (regulators) under the stress-free condition than stress-exposed condition (Fig. 5), suggesting that directional (positive or negative) epistasis formed through a web of regulators and regulatees is a crucial but previously neglected determinant of G-E interactions. Also, we found that some insignificant SNPs by traditional approaches are insignificant because they are negatively regulated by other SNPs. These findings have many practical implications for the genetic editing of *P. euphratica*. For instances, we can activate the expression of positive regulators but repress the expression of negative regulators to augment and amplify the genetic roles of both significant and insignificant loci in promoting stem and root development. Moreover, such genetic manipulation could enable similar growth of the Euphrates poplar under both the salt-exposed and salt-free condition, thus mitigating the environmental stressor.

As compared to mapping main genetic effects and main environmental effects alone, mapping genetic interactions or G-E interactions requires a considerably greater sample size (Zuk et al. 2012; Murcray et al. 2011), which is rarely achieved in practice. However, unlike conventional methods, our model for inferring epistatic, environment-induced networks is much less sample size-reliant. The key step of network inference using our model is to estimate ODE parameters that constitute a system of nLV-based ODEs in equation (5). The precision of ODE parameter estimation depends on the number of time points and the estimation precision of main genetic

effects. Given that their number is much fewer than that of time points, ODE parameters can be reasonably estimated, as shown in our previous simulation study (Jiang et al. 2020). Although our mapping experiments use a modest sample size ($n \approx 100$), main genetic effects of individual SNPs can still be reasonably precisely estimated for the following reasons. First, each member of our mapping populations is repeated with three clonal replicates in two contrast environments, thus totaling over 600 trees in each experiment. Computer simulation shows that one additional replicate of a genotype is, on the whole, equivalent to adding one more genotype in terms of the testing power and precision of parameter estimation (Knapp and Bridges 1990). This suggests that our sample size at work may be at least $n = 600$. Second, the same tree was repeatedly measured at 14 (root length) or 6 time points (stem height), which provides $600 \times 14 = 8,400$ and $600 \times 6 = 3,600$ observation points. Both clonal replicates and repeated measurements can greatly augment mapping information. Third, our experimental trees were well controlled in a homogeneous environment (Fig. S1) so that their phenotyping could be made at high precision. Simulations studies show that measurement errors (and therefore heritability) affect mapping precision and power to a larger extent than sample size (Jiang et al. 2015). Fourth, the main genetic effects are estimated by functional mapping that fits biologically relevant curves of trait growth and the statistically meaningful autocorrelative structure of the residual covariance matrix (Ma et al. 2002; Wu and Lin 2006). Computer simulation shows that functional mapping can accurately estimate time-varying main genetic effects of a SNP even under a modest heritability ($H^2 = 0.05$) and a modest sample size ($n = 100$) (Fig. S10). The accuracy of effect estimation is more sensitive to increasing heritability than sample size; for example, estimation accuracy under $H^2 = 0.10$ and $n = 100$ can be matched for $H^2 = 0.05$ by many more samples, i.e., $n = 400 - 800$, depending on the temporal pattern of genotypic differences. We also find that functional mapping has greater power for QTL detection than static mapping at single time points under the same heritability and sample size, especially when genotypic curves are non-parallel and/or crossover at a point of the growth process (Fig. S10). On the other hand, functional mapping has a low type I error, with false positive rates of < 0.08 under $n = 100$. The additional advantage of functional mapping lies in its capacity to interpolate as many time points as needed for precise network reconstruction.

We have proposed a general framework for reconstructing and use multilayer omnigenic networks to study the causes and consequences of G-E interactions at the macroscopic, mesoscopic, and microscopic levels. The algorithmic aspects of the framework include curve smoothing, variable selection, matrix structuring, and ODE solving, each of which can be improved by introducing the advanced theory and methods of modern applied mathematics and statistics through interdisciplinary collaboration. Although we validate our model using a tree mapping experiment, the application of the model to other organisms including humans is feasible. As one of the biggest human genome projects, GTEx, aimed to study the genetic variation of human diseases across multiple tissues, has accumulated over thousands of donors for which genotype data, transcriptional data on multiple tissues, and histological data have been collected (GTEx Consortium 2015, 2020). We integrate allometric scaling theory (Ye et al. 2020) to express each gene as a function of tissues and estimate net genetic effects of each SNP on tissue-varying gene expression, from which to reconstruct genetic networks across tissues. Another large-scale human genome project, known as the Hammington Heart Study, has collected tens of thousands of male and female subjects who were genotyped and phenotyped for many health-related traits, such as BMI and blood pressures at different ages (Fox et al. 2007; Andersson et al. 2019). Our model can be used to reconstruct multilayer genetic networks to dissect gene-sex interactions for the development of health traits. Together, our model opens up a new avenue to unveil the genetic complexities of how genes interact with environmental change to help the organism better adapt to environmental cues.

Acknowledgements

We thank many members at the Center for Computational Biology for their contributions to collect data used in this manuscript. This work is supported by grant 201404102 from the State Administration of Forestry of China and grant 31700576 from National Natural Science Foundation of China. C.G. was supported by the National Science Foundation under grant NSF DMS-1814876.

Author contributions

Conceptualization and Methodology, R.W.; Computation, Coding, and Visualization: H.W., M.Y., A.D. and L.J.; Experimentation, M.Y., Y.F., X.Z. and W.B.; Writing, R.W.; Revision and Editing: C.G.

DECLARATION OF INTERESTS

The authors declare no competing interests.

References

Allesina, S., and Tang, S. (2012). Stability criteria for complex ecosystems. Nature *483*, 205-208.

Andersson, C., Johnson, A.D., Benjamin, E.J., and Levy D, Vasan, R.S. (2019). 70-year legacy of the Framingham Heart Study. Nat. Rev. Cardiol. *16*, 687–698.

Arnau-Soler, A., Macdonald-Dunlop, E., Adams, M.J., Clarke, T.K., MacIntyre, D.J., Milburn, K., Navrady, L.; Generation Scotland; Major Depressive Disorder Working Group of the Psychiatric Genomics Consortium; Hayward, C. et al. (2019). Genome-wide by environment interaction studies of depressive symptoms and psychosocial stress in UK Biobank and Generation Scotland. Transl. Psychiatry *9*, 14.

Aschard, H. (2016). A perspective on interaction effects in genetic association studies. Genet Epidemiol. *40*, 678–688.

Axelrod, R. and Hamilton, W.D. (1981). The evolution of cooperation. Science *211*, 1390-1396.

Bateson, W. (1907). The progress of genetics since the rediscovery of Mendel's paper. Progressus Rei Botanicae *1*, 368–382.

Boyce, W.T., Sokolowski, M.B., and Robinson, G.E. (2020). Genes and environments, development and time. Proc. Natl. Acad. Sci. U S A. *117*, 23235-23241.

Boyle, E, A., Li, Y.I., and Pritchard, J.K. (2017). An expanded view of complex traits: From polygenic to omnigenic. Cell *169,* 1177-1186.

Busiello, D. M., Suweis, S., Hidalgo, J., and Maritan, A. (2017). Explorability and the origin of network sparsity in living systems. Sci. Rep. *7*, 12323.

Cassaniti, C., Romano, D., and Flowers, T.J. (2012). The response of ornamental plants to saline irrigation water, p. 131–158. In: I. Garcia-Garizabal (ed.) Irrigation: Water management, pollution and alternative strategies. In Tech, Rijeka, Croatia.

Clark, R. T., MacCurdy, R. B., Jung, J. K., Shaff, J. E., McCouch, S. R., Aneshansley, D. J., and Kochian, L. V. (2011). Three-dimensional root phenotyping with a novel imaging and software platform. Plant Physiol. *156*, 455-465.

Costanzo, M., Kuzmin, E., van, Leeuwen, J., Mair, B., Moffat, J., Boone, C., and Andrews, B. (2019). Global genetic networks and the genotype-to-phenotype relationship. Cell *177*, 85-100.

Del, S. A., Balling, R., Hood, L., and Galas, D. (2010). Diseases as network perturbations. Curr. Opin. Biotechnol. *4*, 566-571.

Diouf, I., Derivot, L., Koussevitzky, S., Carretero, Y., Bitton, F., Moreau, L., and Causse, M. (2020). Genetic basis of phenotypic plasticity and genotype × environment interactions in a multi-parental tomato population. J. Exp. Bot. *71*, 5365-5376.

Dunbar, R. I. M. (1992). Neocortex size as a constraint on group size in primates. J. Hum. Evol. *22*, 469-493.

El-Soda, M., Malosetti, M., Zwaan, B. J., Koornneef, M., and Aarts, M. G. (2014). Genotype× environment interaction QTL mapping in plants: lessons from Arabidopsis. Trends Plant Sci. *19*, 390-398.

Esposito, G., Azhari, A., and Borelli, JL. (2018). Gene × Environment interaction in developmental disorders: Where do we stand and what's next? Front. Psychol. *9*, 2036.

Félix, M.A., and Barkoulas, M. (2015). Pervasive robustness in biological systems. Nat. Rev. Genet. *16*, 483–496.

Fox, C.S., Heard-Costa, N., Cupples, L.A., Dupuis, J., Vasan, R.S., and Atwood, L.D. (2007). Genome-wide association to body mass index and waist circumference: the Framingham Heart Study 100K project. BMC Med. Genet. *8 Suppl 1*, S18.

Gottlieb, G. (2007). Probabilistic epigenesis. Dev. Sci. *10*, 1–11.

Gross, T., Rudolf, L., Levin, S.A., and Dieckmann, U. (2009). Generalized models reveal stabilizing factors in food webs. Science *325*, 747-750.

GTEx Consortium (2015). The Genotype-Tissue Expression (GTEx) pilot analysis: multitissue gene regulation in humans. Science *348*, 648-660.

GTEx Consortium (2020). The GTEx Consortium atlas of genetic regulatory effects across human tissues. Science *369(6509)*, 1318-1330.

Han, S. W., Chen, G., Cheon, M. S., and Zhong, H. (2016). Estimation of directed acyclic graphs through two-stage adaptive Lasso for gene network inference. J. Am. Stat. Assoc. *111*, 1004-1019.

Hui, Z. (2006). The adaptive Lasso and its oracle properties, J. Am. Stat. Assoc. *101*, 1418-1429.

Hunter, D. (2005). Gene–environment interactions in human diseases. Nat. Rev. Genet. *6*, 287–298.

Jenss, R.M., and Bayley, N. (1937). A mathematical method for studying the growth of a child. Hum. Biol. *9*, 556–563.

Jiang, L.B., Liu, J.Y., Zhu, X.L., Ye, M.X., Sun, L.D., Lacaze, X., and Wu, R.L. (2015). 2HiGWAS: A unifying high-dimensional platform to infer the global genetic architecture of trait development. Brief. Bioinform. *16*, 905-911.

Jiang, L.B., Shi, H., Sang, M., Zheng, C., Cao, Y., Zhu, X., Zhuo, X., Cheng, T., Zhang, Q., Wu, R., and Sun, L. (2019). A computational model for inferring QTL control networks underlying developmental covariation. Front. Plant Sci. *10*, 1557.

Jiang, L., Griffin, C. H., and Wu, R. (2020). SEGN: Inferring real-time gene networks mediating phenotypic plasticity. *Comput. Struct. Biotech. J. 18*, 2510–2521.

Kim, B.R., Zhang, L., Berg, A., Fan, J., and Wu, R.. (2008). A computational approach to the functional clustering of periodic gene expression profiles. Genetics *180*, 821–834.

Li, Z.T., and Sillanpaa, M.J. (2015). Dynamic quantitative trait locus analysis of plant phenomic data. Trends Plant Sci. *20*, 822–833.

Li, J., Li, X., Zhang, S., and Snyder, M. (2019). Gene-environment interaction in the era of precision medicine. Cell *177*, 38-44.

Liu, X., Li, Y.I., and Pritchard, J.K. (2019). Trans effects on gene expression can drive omnigenic inheritance. Cell *177*, 1022-1034.

Lobet, G., Pagès, L., and Draye, X. (2011). A novel image-analysis toolbox enabling quantitative analysis of root system architecture. Plant Physiol. *157*, 29-39.

Lyra, D.H., Virlet, N., Sadeghi-Tehran, P., Hassall, K.L., Wingen, L.U., Orford, S., Griffiths, S., Hawkesford, M.J., and Slavov, G.T. (2020). Functional QTL mapping and genomic prediction of

canopy height in wheat measured using a robotic field phenotyping platform. J. Exp. Bot. *71*(6), 1885-1898.

Ma, C.X., Casella, G., and Wu, R. (2002). Functional mapping of quantitative trait loci underlying the character process: a theoretical framework. Genetics *161*, 1751-1762.

May, R. M. (1972). Will a large complex system be stable? Nature *238*, 413–414.

McAllister, K., Mechanic, L.E., Amos, C., Aschard, H., Blair, I.A., Chatterjee, N., Conti, D., Gauderman, W.J., Hsu, L., Hutter, C.M., et al. (2017). Current challenges and new opportunities for gene-environment interaction studies of complex diseases. Am. J. Epidemiol. *186*, 753-761.

McNamara, J.M. (2013). Towards a richer evolutionary game theory. J. R. Soc. Interface *10*, 20130544.

Melo, D., Porto, A., Cheverud, J.M., and Marroig, G. (2016). Modularity: genes, development and evolution. *Annu. Rev. Ecol. Evol. Syst*. 47, 463-486.

Mulligan, M.K., Mozhui, K., Prins, P., and Williams, R.W. (2017). GeneNetwork: A toolbox for systems genetics, Methods Mol. Biol. *1488*, 75-120.

Murcray, C.E., Lewinger, J.P., Conti, D.V., Thomas, D.C., and Gauderman, W.J. (2011). Sample size requirements to detect gene-environment interactions in genome-wide association studies. Genet. Epidemiol. *35*, 201–210.

Sackton, T.B., and Hartl, D.L. (2016). Genotypic context and epistasis in individuals and populations. Cell *166*, 279-2872016.

Shannon, M.C., and Grieve, C.M. (1999). Tolerance of vegetable crops to salinity, Scientia Horticulturae 78, 5-38.

Smith, J.M., and Price, G.R. (1973). Logic of animal conflict. Nature *246*, 15-18.

Soleimani, A., Etermad, V., Calagari, M., Namiranian, M., and Shirvani, A. (2014). Influence of climatic factors on fruit morphological traits in Populus euphratica Oliv. Ann. For. Res. *57*, 31-38.

Sparrow, D.B., Chapman, G., Smith, A.J., Mattar, M.Z., Major, J.A., O'Reilly, V.C., Saga, Y., Zackai, E.H., Dormans, J.P., Alman, B.A., et al. (2012). A mechanism for gene-environment interaction in the etiology of congenital scoliosis. Cell *149*, 295-306.

Sulc, J., Mounier, N., Günther, F., Winkler, T., Wood, A.R., Frayling, T.M., Heid, I.M., Robinson, M.R., and Kutalik, Z. (2020). Quantification of the overall contribution of gene-environment interaction for obesity-related traits. Nat. Commun. *11*, 1385.

Sun, L.D., Ye, M.X., Hao, H., Wang, N.T., Wang, Y.Q., Cheng, T.R., Zhang, Q.X., and Wu, R.L. (2014). A model framework for identifying genes that guide the evolution of heterochrony. Mol. Biol. Evol. *31*, 2238-2247.

Tam, V., Patel, N., Turcotte, M., Bossé, Y., Paré, G., and Meyre, D. (2019). Benefits and limitations of genome-wide association studies. Nat. Rev. Genet. *20*, 467–484.

Thomas, D. (2010). Gene-environment-wide association studies: emerging approaches. Nat. Rev. Genet. *11(4)*, 259–272.

Tibshirani, R. (1996). Regression shrinkage and selection via the Lasso. J. Roy. Stat. Soc. Ser. B (Methodological) *58*, 267-288.

Verweij, N., Benjamins, J.W., Morley, M.P., van de Vegte, Y.J., Teumer, A., Trenkwalder, T., Reinhard, W., Cappola, T.P., van de Harst, P. (2020). The genetic makeup of the electrocardiogram. Cell Syst. *11*, 229-238.e5.

Vijesh, N., Chakrabarti, S., and Sreekumar, J. (2013). Modeling of gene regulatory networks: A review. J. Biomed. Sci. Eng. *6*, 223-231.

von Neumann J, Morgenstern O. Theory of Games and Economic Behavior. Princeton University Press Princeton, New Jersey, 1946.

Wang, H., and Leng, C. (2008). A note on adaptive group lasso, Comput. Stat. Data Anal. *52(12)*, 5277-5286.

Wang, H., Zhang, F., Zeng, J., Wu, Y., Kemper, K.E., Xue, A., Zhang, M., Powell, J.E., Goddard, M.E., Wray, N.R., et al. (2019). Genotype-by-environment interactions inferred from genetic effects on phenotypic variability in the UK Biobank. Sci Adv. *5*, eaaw3538.

Wang, Y.Q., Xu, M., Wang, Z., Tao, M., Zhu, J., Wang, L., Li, R., Berceli, S.A., and Wu, R. (2012). How to cluster gene expression dynamics in response to environmental signals. Brief. Bioinform. *13*, 162–174.

Wild, A. (1988). Russell's soil conditions and plant growth. 11th edn. Harlow, Longman.

Wu, C., and Cui, Y. (2013). A novel method for identifying nonlinear gene-environment interactions in case-control association studies. Hum. Genet. *132*, 1413-1425.

Wu, C., Zhong, P.S., and Cui, Y. (2018). Additive varying-coefficient model for nonlinear gene-environment interactions. Stat. Appl. Genet. Mol. Biol. *17*, https://www.j/sagmb.2018.17.issue-2/sagmb-2017-0008/sagmb-2017-0008 .xml.

Wu, R.L., Ma, C.X., Lin, M., and Casella, G. (2004). A general framework for analyzing the genetic architecture of developmental characteristics. Genetics *166*, 1541-1551.

Wu, R.L. (1998). The detection of plasticity genes in heterogeneous environments. Evolution *52*, 967-977.

Wu, R.L., and Lin, M. (2006). Functional mapping—how to map and study the genetic architecture of dynamic complex traits. Nat. Rev. Genet. *7*, 229-237.

Wang, Y.X., and Huang, H. (2014). Review on statistical methods for gene network reconstruction using expression data, J. Theor. Biol. *362*, 53-61.

Ye, M.X., Jiang, L.B., Chen, C., Zhu, X., Wang, M., and Wu, R. (2019). np2QTL: networking phenotypic plasticity quantitative trait loci across heterogeneous environments. Plant J. *99*, 796-806.

Zhang, M.M., Xu, F., Li, H., Shi, C.Z., Wang, D.Y., Bo, W.H., Ye, M.X., Jiang, L.B., Liang, D., and Wu, R. (2017). The genetic architecture of shoot-root covariation during seedling emergence of a dessert tree, Populus euphratica. Plant J. *90*, 918-928.

Zhang, Z., Chen, Y., Zhang, J., Ma, X., Li, Y., Li, M., and Olson, M. S. (2020). Improved genome assembly provides new insights into genome evolution in a desert poplar (*Populus euphratica*). Mol. Ecol. Res. 20. doi: 10.1111/1755-0998.13142.

Zhao, W., Hou, W., Littell, R.C., and Wu, R.L. (2005). Structured antedependence models for functional mapping of multivariate longitudinal traits. Stat. Methods Mol. Genet. Biol. *4*, Article 33.

Zuk, O., Hechter, E., Sunyaev, S.R., and Lander, E.S. The mystery of missing heritability: Genetic interactions create phantom heritability. Proc. Natl. Acad. Sci. U S A. *109*, 1193-1198.

Star*Methods

RESOURCE AVAILABILITY

Lead contact

Further information and requests for resources and reagents should be directed to and will be fulfilled by the lead contact, Rongling Wu (rwu@phs.psu.edu).

Data and code availability

The data and code uploaded at https://github.com/LiboJiang/EuphratesGWEISNetwork can be freely downloaded and used by researchers worldwide. These code and data can also be requested directly from the corresponding author.

METHOD DETAILS

A general design of experiment

Consider a linkage or association mapping population that is grown under two contrast conditions Y and Z to study gene-environment interactions. This population has been genotyped, producing a high throughput of genome-wide SNPs (say S) for genetic mapping. All n members of the population are phenotyped for a complex trait at a series of time points during ontogeny. We expect that the developmental trajectory of the trait is different between the two environments, but the significance of such a difference should be tested by statistical analysis. Let $\mathbf{y}_i = (y_i(t_1), \ldots, y_i(t_T))$ and $\mathbf{z}_i = (z_i(t_1), \ldots, z_i(t_T))$ denote the phenotypic values of a complex trait measured for the ith mapping member at time schedule $(t_1, \ldots, t_T)$ in environment Y and Z, respectively. We formulate a joint likelihood for these observations, expressed as

$$L(\mathbf{y}, \mathbf{z}) = \prod_{i=1}^{n} f\left(\mathbf{y}_i, \mathbf{z}_i; \boldsymbol{\mu}_y, \boldsymbol{\mu}_z, \Sigma\right) \quad (1)$$

where $f(\cdot)$ is a bivariate T-dimensional normal distribution with mean vector $\boldsymbol{\mu} = (\boldsymbol{\mu}_y, \boldsymbol{\mu}_z)$ and covariance matrix $\boldsymbol{\Sigma}$. We assume that the time-dependent change of the trait studied can be

described by a biologically meaningful mathematical function, such as growth equation, or a nonparametric smoothing function. If trait trajectories are different between two environments, parameters that describe the function of trait change should be environment specific. Because the covariance matrix contains longitudinal information, we use an autoregressive model, such as the bivariate first-order structured antedependence (biSAD(1)) model (Zhao et al. 2005), to fit the structure of the covariance, increasing the model's parsimony. Under the null hypothesis that there is no environment-specific difference, i.e., $\boldsymbol{\mu}_y = \boldsymbol{\mu}_z$, we formulate a second likelihood. The calculated log-likelihood ratio (LR) can be used as a test statistic to test whether trait development is different between two environments.

The above testing procedure is used to test environment-dependent differences in the overall mean of all progeny. A similar procedure is implemented to test whether a specific progeny differs in trait development between two environments. If the extent and pattern of such a difference depends on progeny, this implies that there exist genotype-environment interactions. Traditional reductionist thinking is to identify individual significant QTLs that are expressed differently between environments, but it may provide limited insight into the genetic machineries that shape genotype-environment interactions and their evolutionary consequences. We argue that the design described above allows us to chart a comprehensive genetic atlas for phenotypic response to environmental change.

Bivariate functional mapping

We implement bivariate functional mapping (biFunMap) to characterize whether and how a specific locus determines the developmental trajectories of the complex trait expressed over environments. Consider a SNP s at which the j_s-th ($j_s = 1, \ldots, J_s$) genotype has n_{j_s} observations. The bFunMap model is built on the likelihood of phenotypic values at this SNP, expressed as

$$L_1(\mathbf{y}, \mathbf{z}) = \prod_{j_s=1}^{J_s} \prod_{i=1}^{n_{j_s}} f_{j_s}\left(\mathbf{y}_i, \mathbf{z}_i; \boldsymbol{\mu}_{j_s}^{y}, \boldsymbol{\mu}_{j_s}^{z}, \Sigma\right) \quad (2)$$

where $f_{j_s}(\cdot)$ is a $2T$-dimensional multivariate normal distribution with mean vector $\boldsymbol{\mu}_{j_s}^{y}$ = $(\mu_{j_s}^{y}(t_1), \ldots, \mu_{j_s}^{y}(t_T))$ in environment X and $\boldsymbol{\mu}_{j_s}^{z}$ = $(\mu_{j_s}^{z}(t_1), \ldots, \mu_{j_s}^{z}(t_T))$ for environment Y and covariance matrix Σ. Functional mapping models time-specific means in $\boldsymbol{\mu}_{j_s}^{y}$ and $\boldsymbol{\mu}_{j_s}^{z}$ by biologically meaningful mathematical equations (e.g., growth equations) that describe the developmental trajectories of the trait expressed in the two environments. To reflect environment-dependent differences, we use two sets of mathematical parameters, each related to trait development in a different environment. Because Σ has an autoregressive structure, functional mapping models its time-varying variances and covariances by bSAD(1) (Zhao et al. 2005).

We implemented the Nelder-Mead simplex algorithm to obtain the maximum likelihood estimates (MLEs) of the model parameters constituting the likelihood (2). After trait development-related parameters are estimated, we can calculate the genetic standard deviation of a SNP *s* for the trait at any time point *t* in environment *k* (*k* = X, Y), expressed as

$$g_s^k(t) = \sqrt{\frac{1}{n}\sum_{j_s=1}^{J_s} n_{j_s}\left(\mu_{j_s}^k(t)\right)^2 - \left(\frac{1}{n}\sum_{j_s=1}^{J_s} n_{j_s}\,\mu_{j_s}^k(t)\right)^2} \tag{3}$$

which describes the genetic effect of this SNP on trait development. To test the statistical significance of this SNP, we formulate the following hypotheses:

$$\begin{aligned} &\mathrm{H}_0\text{: } \boldsymbol{\mu}_{j_s}^{y} \equiv \boldsymbol{\mu}_y \cap \boldsymbol{\mu}_{j_s}^{z} \equiv \boldsymbol{\mu}_z \\ &\mathrm{H}_1\text{: } \boldsymbol{\mu}_{j_s}^{y} \neq \boldsymbol{\mu}_y \cup \boldsymbol{\mu}_{j_s}^{z} \neq \boldsymbol{\mu}_z \end{aligned} \tag{4}$$

under each of which we calculate the likelihood values and use them to calculate the LR (likelihood ratio) value as a test statistic. Permutation tests can be used to determine the genome-wide critical threshold.

After a SNP is tested to be significant, we need to further test whether it affects trait development in both environments or if its significance is environment-specific. This can be done by formulating the following hypotheses:

$$\begin{aligned} &H_0: \boldsymbol{\mu}_{j_s}^{y} \equiv \boldsymbol{\mu}_y \\ &H_1: \boldsymbol{\mu}_{j_s}^{y} \neq \boldsymbol{\mu}_y \end{aligned} \tag{4A}$$

to test whether the SNP only affects trait development in environment Y, and

$$\begin{aligned} &H_0: \boldsymbol{\mu}_{j_s}^{z} \equiv \boldsymbol{\mu}_z \\ &H_1: \boldsymbol{\mu}_{j_s}^{z} \neq \boldsymbol{\mu}_z \end{aligned} \tag{4B}$$

to test whether the SNP only affects trait development in environment Z. If the null hypotheses of tests (4A) and (4B) are both rejected, then this means that this SNP "pleiotropically" affects trait development in both environments. All the steps described above are a standard procedure of traditional genetic mapping for identifying key QTLs, but lacking a capacity to encapsulate all loci into an omnigenic network that shapes phenotypic variation.

Genetic network reconstruction: sparsity, stability and causality

All genetic loci work together as a cohesive whole to determine trait phenotype. We argue that, in this whole, each locus exerts its own effect and/or regulates other loci that directly participate in trait control. This argument is essentially equivalent to arguing that the net genetic effect of a locus, observed by a marginal effect-based model, contains this locus' direct effect and the indirect effects of other loci that regulate it through various pathways. The relative contributions of direct and indirect effect can be explained through dynamic lens of evolutionary game theory (Smith and Price 1973). Classical game theory suggests that a rational player strives to maximize its payoff based using its own independent strategy whose selection is dependent on the strategies of several interacting players, a process that continues until the Nash equilibrium is reached (Nash 1950). By combining game theory and evolution, evolutionary game theory studies these two different strategies, but does not rely upon the rationality assumption. Instead, the notion of evolutionarily stable strategy is used as a refined Nash equilibrium. We extend

evolutionary game theory to a dynamic representation that allows independent and dependent strategies to be modeled by a system of nonlinear Lotka-Volterra (nLV) equations.

Let $\mathbf{g}_s^y = (g_s^y(t_1), \ldots, g_s^y(t_T))$ and $\mathbf{g}_s^z = (g_s^z(t_1), \ldots, g_s^z(t_T))$ denote two vectors of the overall genetic effect of SNP *s* on trait development in environments X and Y, respectively. According to evolutionary game theory, we decompose the net genetic effect of a SNP into its independent effect component and dependent effect component, which is described by an nLV-based ordinary differential equation (ODE), i.e.,

$$\dot{g}_s^k(t) = Q_s^k(g_s^k(t); \Theta_s^k) + \sum_{s'=1, s' \neq s}^{S} Q_{ss'}^k\left(g_{s'}^k(t); \Theta_{ss'}^k\right) \quad (5)$$

where $\dot{g}_s^k(t)$ is the derivative of the net genetic effect of SNP *s* on trait development at time *t* in environment *k*, $Q_s^k(\cdot)$ is a time-varying function that characterizes the independent genetic effect of SNP *s* that occurs when it is assumed to be in isolation, $Q_{ss'}^k(\cdot)$ is a time-varying function that characterizes the dependent genetic effect of SNP *s* that arises from the influence of another SNP s' on it, and Θ_s^k and $\Theta_{ss'}^k$ are a set of parameters that fit the independent and dependent functions, respectively. Since both time-varying independent and dependent effects do not follow an explicit equation, we implement a nonparametric smoothing approach, such as Legendre Orthogonal Polynomials (LOP). LOP has been shown to be very flexible for fitting many arbitrary forms of curves (Das et al. 2012; Jiang et al. 2016).

According to network theory, the number of entities linked with a particular entity in a network is limited, depending on the size of the network (Dunbar 1992). This suggests that a network may be sparse in links. This is thought to be a desirable property for a community to buffer against perturbations and maintain the community's stability (May 1972; Gross et al. 2009; Allesina and Tang 2012; Busiello et al. 2017). We thus incorporate LASSO-based variable selection (Tibshirani et al. 1996; Hui 2006; Wang and Leng 2008) to select a small set of SNPs that are the most significant for a given SNP. This can be done by regressing the net genetic effect of a SNP on those of all other SNPs across time points. In practice, the number of SNPs

may be so much larger than the number of time points that variable selection may perform incorrectly. In this case, we may interpolate additional values on the fitting curve of genetic effects over time as a multiple regression model.

Equation (5) is regarded as a full model because each SNP is connected to all other SNPs. Through variable selection, this full model is reduced to include a small number of the most significant SNPs related to each SNP. Let d_s ($d_s << S$) denote such a number for SNP s, which replaces S in the second term of equation (5) to build up a sparse ODE. Because we genotype S SNPs in the mapping study, there are S such sparse ODEs that comprise an nLV system.

We formulate a likelihood function for estimated genetic effects of S SNPs by biFunMap, under which ODE parameters are estimated by implementing the fourth-order Kunge-Kutta algorithm. The maximum likelihood estimation (MLEs) problem for ODE parameters (arrayed in Θ_s^k and $\Theta_{ss'}^k$) is a convex optimization so that the nLV system established by these MLEs may be regarded as being stable. By plugging the MLEs of the ODE parameters into the dependent term of equation (5), we can estimate the independent effect components for individual SNP pairs. For a pair of SNPs, A and B, we can estimate the interdependent effect of A due to B and the interdependent effect of B due to A, and these reciprocal estimates, which can be positive or negative with any value, establish a causal relationship between SNPs A and B. We code the independent genetic effects of different SNPs as nodes and the dependent genetic effects of SNP pairs as edges in a graph. Obviously, this graph represents a maximally informative network filled with bidirectional, signed, and weighted interactions. Taken together, genetic networks reconstructed from the above procedure meet the three required properties of a network, sparsity, stability, and causality.

A multilayer network inferred from high-dimensional genotype data

For current mapping studies, genotyping tens or hundreds of thousands of SNPs is not uncommon. As discussed above, it is impossible for a SNP to connect all other SNPs at the same time, thus a LASSO-based approach is implemented to choose a small set of the most significant SNPs that are linked with a given SNP. However, despite the formulation of a sparse ODE for each SNP, statistical estimates of a high- or ultrahigh-dimensional nLV system are

computationally prohibited. We introduce developmental modularity theory (Melo et al. 2016) to resolve this issue. This theory states that the complex system can be divided into distinct communities within which components are connected more tightly with each other than those from other communities. Many studies show that the existence of network communities facilitates the stability and robustness of a complex system (May 1972; Gross et al. 2009; Allesina and Tang 2012; Busiello et al. 2017). In a GWAS of a trait measured at 500 time points, Verweij et al. (2020) found that SNPs are clustered based on the temporal similarity of their genetic effects over all time points. This implies that we can divide a large genetic network into distinct network communities by clustering all SNPs into different modules, each of which represents a different network community.

To reflect the time-varying pattern of genetic effects, we implement bivariate functional clustering (biFunClu) (Wang et al. 2010) to divide all *S* SNPs into different modules according to how they affect trait development in environment Y and Z, described by $\mathbf{g}_s^y = (g_s^y(t_1), \ldots, g_s^y(t_T))$ and $\mathbf{g}_s^z = (g_s^z(t_1), \ldots, g_s^z(t_T))$, respectively. BFunClu is formulated on the basis of a mixture-based likelihood model, expressed as

$$L_2(\mathbf{g}_y, \mathbf{g}_z) = \prod_{s=1}^{S} \sum_{l=1}^{L} [\pi_l f_l(\mathbf{g}_s^y, \mathbf{g}_s^z; \mathbf{u}_l^y, \mathbf{u}_l^z, \Sigma_g)] \quad (6)$$

where *L* is the number of modules, π_l is a prior probability representing the proportion of module *l*, and $f_l(\cdot)$ is the 2*T*-dimensional multivariate normal distribution with mean vector $\mathbf{u}_l^y = (u_l^y(t_1), \ldots, u_l^y(t_T))$ for environment X and $\mathbf{u}_l^z = (u_l^z(t_1), \ldots, u_l^z(t_T))$ for environment Y and covariance matrix Σ_g. We implement a LOP-based nonparametric model to fit the structure of $\mathbf{u}_l^y$ and $\mathbf{u}_l^z$ and bSAD(1) to fit the structure of Σ_g.

We develop a hybrid of the EM and simplex algorithms to maximize the likelihood (6). An optimal number of mixture components (i.e., modules) is determined according to AIC. The module (*l*) to which a specific SNP *s* belongs can be determined on the basis of the estimate of the posterior probability, expressed as

$$\Pi_{l|s} = \frac{\pi_l f_l\left(\mathbf{g}_s^y, \mathbf{g}_s^z; \mathbf{u}_l^y, \mathbf{u}_l^z, \Sigma_g\right)}{\sum_{l'}^{L} \pi_{l'} f_{l'}\left(\mathbf{g}_s^y, \mathbf{g}_s^z; \mathbf{u}_{l'}^y, \mathbf{u}_{l'}^z, \Sigma_g\right)} \quad (7)$$

A SNP is assigned to a module if the posterior probability of this SNP ($\Pi_{l|s}$) within this module is larger than those in any other modules.

The biFunClu model allows us to detect multiple network communities from a huge network. The interconnections of network communities can be made by reconstructing an inter-module network based on the overall genetic effects of SNPs from the same modules using the above procedure. The number of modules, usually considerably smaller than the number of SNPs, makes it feasible to reconstruct a so-called coarse-grained or macroscopic genetic network at the module level (Chen et al. 2019). We expect that the number of SNPs within a module reduces dramatically to a level at which a SNP-SNP interaction network can be computationally reconstructed. A genetic network at the SNP level is called the fine-grained or microscopic genetic network. If a given module is still too large to be handled by variable selection, we can implement biFunClu to classify this module into distinct submodules. Similarly, a submodule can be classified into distinct sub-submodules, and this procedure continued until a unit is small enough to be properly handled. We call genetic networks reconstructed with submodules or sub-submodules, etc. mesoscopic networks. One macroscopic network, with each community composed of multiple mesoscopic or microscopic networks, forms a multilayer genetic network, from which we can characterize the roadmap of how each SNP affects trait phenotype through direct and/or indirect paths.

A comparative analysis of genetic networks under two environments

We reconstruct two multilayer networks each for an environment. Environment-dependent differences in network structure and organization reflect the strength and pattern of G-E interactions for trait control. Network analysis can characterize two different ways in which G-E interactions occur: (1) environment-induced change in main (independent) genetic effects and (2) environment-induced in epistatic (dependent) effects. By comparing how much individual nodes differ between two environments, we can determine the role of main effects in mediating G-E

interactions. Similarly, the environment-dependent comparison of edges that connect a pair of nodes can reveal the contribution of epistatic effects to G-E interactions. Previous quantitative genetic models could only identify G-E interactions in terms of main (net) genetic effects, failing to extract gene by gene by environment interactions. Our networks can decipher how directed epistasis causes gene-environment interactions. Instead of using a conventional linear model, we study G-E interactions based on a system of nLV equations. A nonlinear model can better unravel the reality of interactions between genes and the environment (Gottlieb 2007; Félix and Barkoulas 2015). Given that our multilayer networks cover a complete set of genome-wide loci and their existing interactions, this model provides a tool to analyze GWEIS data.

EXPERIMENTAL DETAILS

Construction of a full-sib linkage mapping population

We sampled two healthy wild trees of dioecious Euphrates poplar from its natural desert distribution in Korla, Xijiang Province of the northeastern China, and crossed them to generate a full-sib family. We germinated seeds from the full-sib family into seedlings to establish a mapping population with 106 F_1 hybrids. From this population, 8,305 good-quality SNPs were genotyped to construct a high-density linkage map with a total length of 4,575 cM covering the 19 Populus chromosomes. A detailed procedure of marker genotyping and map construction was given in Zhang et al. (2017).

Part of this mapping population (106 F_1 hybrids) were planted with three clonal replicates under two contrasting treatments. We cultivated uniform buds (about 10 mm, 4-6 blades) from each F_1 seedling in individual grass tubes (40 mm in diameter and 400 mm in length) under a sterile culture condition. The tubes contain 260 ml rooting media, laid out in a phytotron set at 16h-day/8h-night cycle, 26°C day and night with 800μmol m-2 s-1 photosynthetically active radiation. Compared with the control treatment, the salt-stress treatment contains 0.1% NaCl in the media. Thus, the cultivation of the same clone in these two treatments allows us to investigate how Euphrates poplar genotypes respond to saline stress and map genotype-environment interactions.

Buds cultivated in the media sprout into stems above ground and roots below ground. We monitored the dynamic trajectories of adventitious root growth in the tubes by building a 360° camera system for root phenotype (Clark et al. 2011) (Fig. S1). This system took a picture every 15° as the disk rotated. Sprouts first appeared on the 13th day after being cultivated in the tubes. The root images were collected repeatedly for each clonal replicate once every 5 days until the 78th day when shoots and roots filled the tubes (Fig. S1). The length of each root was measured using the ImageJ plug in SmartRoot software (Lobet et al. 2011). We calculated the total length of all adventitious roots emerging from the buds to study G-E interactions of a complex trait.

Growth traits generally follow an S-shaped curve, which can be described by a logistic growth equation. In our case, the measurement of root growth was stopped when the tubes had no space for the root to expand. As such, root growth in the tubes may still be in its early growth stage and may not yet have reached its asymptotic growth stage. Jenss and Bayley (1937) proposed a growth equation to model child growth, in a situation similar to ours. Based on the idea of Jenss-Bayley model, we derive a modified logistic growth equation as follows:

$$g(t) = \frac{a}{1 + be^{-rt}} - ce^{-dt} \tag{8}$$

which is a combination of the logistic growth equation and the decreasing exponential function that allows for decelerating growth during the early growth stage, where a is the asymptotic growth, b is the parameter related to initial growth, r is the relative growth rate, and c and d are two parameters that determine the pattern of decelerating growth.

Construction of a natural GWAS population

We sampled 560 wild trees of desert-adapted Euphrates poplar from its natural distribution in Korla, Xijiang Province of the northeastern China, to establish a GWAS population. These sampled trees are each apart from the others by at least 50 meters. From their upper canopies, we collected two-year-old winter dormant branches and water-cultured them at the greenhouse of Beijing Forestry University. At least 5 cm-long branches containing axillary buds were cut and sterilized using a 70% alcohol and 1% sodium hypochlorite solution. Through several steps of callus induction from these shoot segments, we obtained multiple clonal copies for a portion of

sampled wild trees (genotypes). As a pilot study, we planted 121 genotypes in salt-free (control) culture and 86 genotypes in salt-exposed (stress) culture (containing 0.1% NaCl) with three or more clonal replicates. Note that all stressed genotypes are included in the control treatment. Starting 20 days after culture, we measured stem heights for each tree once every 20 days during the 120 days of culture. Thus, we made our measurements at a total of six evenly-spaced time points. Like root growth, stem growth is a good predictor of salt resistance (Wild 1988; Shannon and Grieve 1999; Cassaniti et al. 2012).

Stem heigh growth follows a logistic curve. A growth curve is determined by key development events and timing, which can be quantified by heterochronic parameters (Sun et al. 2014). We calculated four heterochronic parameters, including the timing of maximum growth rate (t_I = logb/r), relative growth rate (r), and the length of linear growth ($\Delta = T_d - T_a$, with $T_d = \log(2+\sqrt{3})b/r$, the timing of maximum acceleration, and $T_a = \log(2-\sqrt{3})b/r$, the timing of maximum deceleration). These parameters are used to reveal the pattern of trait development.

In total, we genotyped 6,978,931 SNPs for this GWAS population. After excluding minor allele-frequency SNPs and those deviating from Hardy-Weinberg equilibrium, 241,990 high-quality SNPs remained for subsequent association analysis. Based on these remaining SNPs, we used fastStructure software (Raj et al. 2014) to determine the optimal number of subgroups among 121 genotypes. The result from this population structure analysis suggests that no subgroups occur in our GWAS population for the salt-resistant experiment.

Figure Legends

Figure 1 Bivariate functional mapping for identifying QTLs that govern root growth trajectories in the fub-sib family of Euphrates poplar. (**A**) Plots of total adventitious root lengths for 106 F_1 progeny (thin lines) grown in salt-free (control) and salt-stress tubes during the early ontogeny of juvenile trees. The mean curve of the F_1 progeny is fitted by a combination of the logistic growth equation (solid thick line) and decreasing exponential equation (slashed thick line). Based on the logistic equation, the timing of maximum growth rate (t_I) and the length of linear growth (Δ), expressed as the difference between the timing of maximum deceleration (T_d) and the timing of maximum acceleration (T_a). (**B**) Manhattan plot of log-likelihood ratios (LR) against different chromosomes estimated by bivariate functional mapping. Horizontal lines represent the critical thresholds of testcross markers (red line) and intercross markers (blue line) determined from 1000 permutation tests. Many QTLs detected reside at the genomic region of candidate genes (Table S1). Three insignificant SNPs highlighted will be further analyzed from the perspective of genetic networks. (**C**) Genetic effect curves of 33 QTLs, plus three randomly chosen insignificant SNPs, identified from the Manhattan plot, expressed in control (blue) and stress conditions (red).

Figure 2 Identification of network communities from large scale genetic networks for root growth in Euphrates poplars. (**A**) Genetic effect curves of 17 representative modules in control (blue) and stress conditions (red) chosen from a total of 400 gene modules detected by bivariate functional clustering. BIC analysis shows 400 as an optimal number of modules. (**B**) Macroscopic genetic networks among 400 modules reconstructed by the mean effect values of each module under control and stress conditions where red and blue arrowed lines stand for activation and inhibition, with the thickness of lines proportional to the strength of regulation, respectively. Modules containing QTLs are highlighted. The distribution of the number of outgoing links and incoming links across 400 modules under control (blue, upper) and stress conditions (red, lower) is given between the control and stress networks.

Figure 3 Microscopic genetic networks at the SNP level for module M177 (**A**) and M178 (**B**) under control and stress conditions, where red and blue arrowed lines stand for activation and

inhibition, with the thickness of lines proportional to the strength of regulation, respectively. QTLs are highlighted. The distribution of the number of outgoing links and incoming links across SNPs under control (blue, upper) and stress conditions (red, lower) is given between the control and stress networks.

Figure 4 Mesoscopic genetic networks among eight submodules of module M22 and microscopic genetic networks among 12 SNPs from submodule 6 under control and stress conditions, where red and blue arrowed lines stand for activation and inhibition, with the thickness of lines proportional to the strength of regulation, respectively. The submodule containing the QTL is highlighted within the mesoscopic networks and the QTL is highlighted within the microscopic networks. The distribution of the number of outgoing links and incoming links across submodules or SNPs under control (blue, upper) and stress conditions (red, lower) is given between the control and stress networks.

Figure 5 Genetic effect curves of two QTLs from module M177 (**A**), three QTLs from module M178 (**B**), and one QTL from module 22 (**C**) under control and stress conditions. The net genetic effect of a QTL (slash line) is decomposed into the independent effect (red line) and dependent effects (blue lines) received from other SNPs.

Figure 6 Microscopic genetic networks at the SNP level for QTL-absent modules M114 (**A**) and M364 (**B**) under control and stress conditions. Red and blue arrowed lines stand for activation and inhibition, with the thickness of lines proportional to the strength of regulation, respectively. The effect curves of two insignificant SNPs from each module are given between the control and stress networks. The net genetic effect of a QTL (slash line) is decomposed into its independent effect (red line) and dependent effects (blue lines) received from other SNPs.

Figure 1

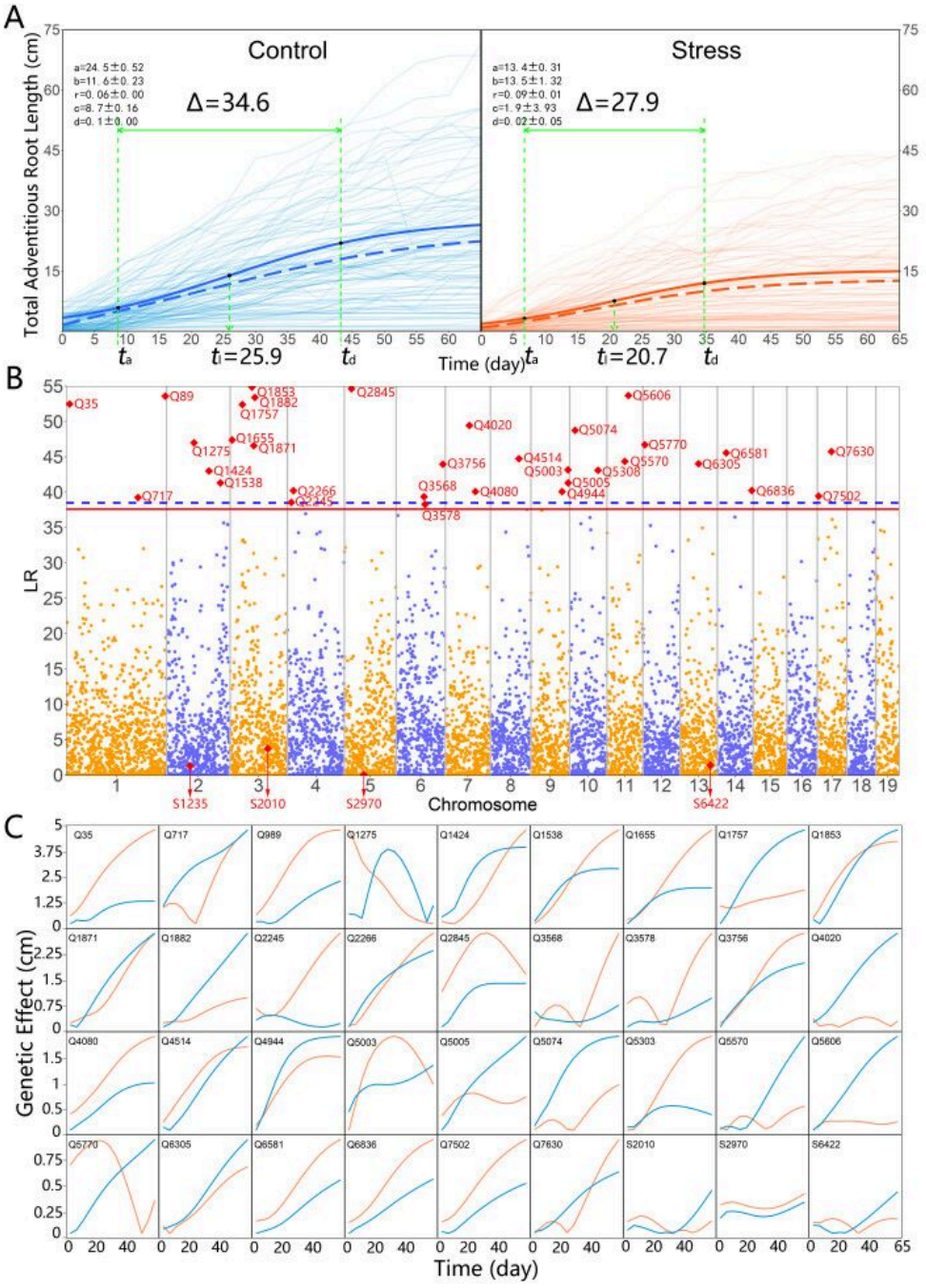
A
Control
Stress
Δ=34.6
Δ=27.9
Total Adventitious Root Length (cm)
Time (day)
B
LR
Chromosome
C
Genetic Effect (cm)
Time (day)

Figure 2

Figure 3

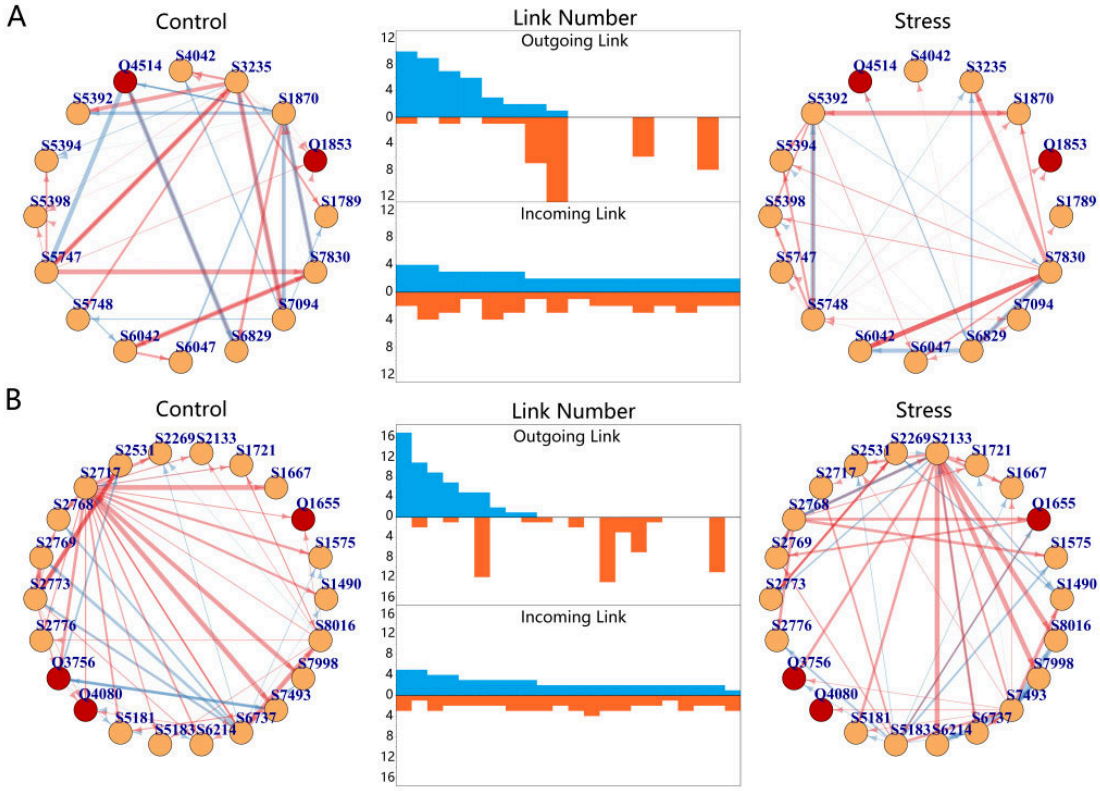
A
Control
Link Number
Outgoing Link
Incoming Link
Stress
Q4514
S4042
S3235
S5392
S1870
Q1853
S5394
S1789
S5398
S5747
S7830
S5748
S7094
S6042
S6047
S6829
B
Control
Link Number
Outgoing Link
Incoming Link
Stress
S2269
S2133
S2531
S1721
S2717
S1667
S2768
Q1655
S2769
S1575
S2773
S1490
S2776
S8016
Q3756
S7998
Q4080
S7493
S5181
S6737
S5183
S6214

Figure 4

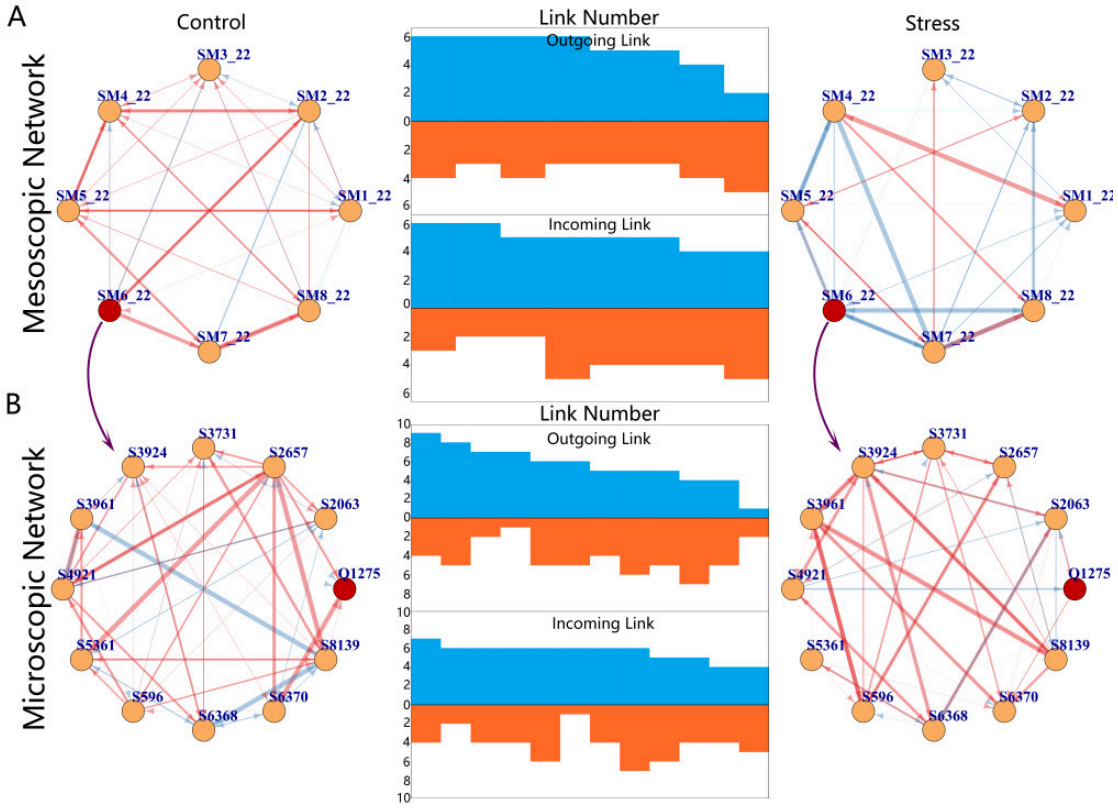
A
Control
Mesoscopic Network
SM3_22
SM4_22
SM2_22
SM5_22
SM1_22
SM6_22
SM8_22
SM7_22
Link Number
Outgoing Link
Incoming Link
Stress
B
Microscopic Network
S3731
S3924
S2657
S3961
S2063
S4921
Q1275
S5361
S8139
S596
S6370
S6368

Figure 5

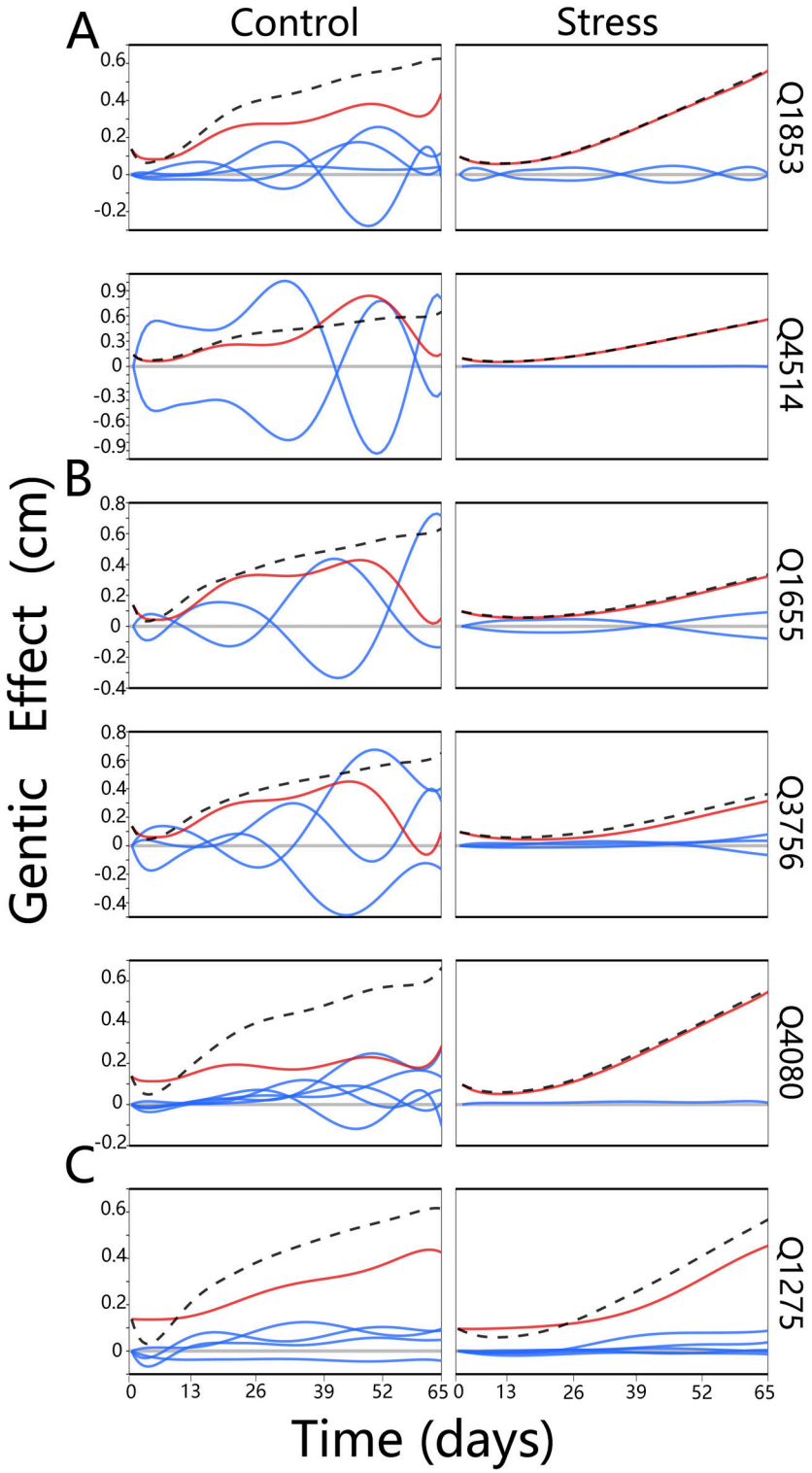
A
Control
Stress
Q1853
Q4514
B
Q1655
Q3756
Q4080
C
Q1275
Gentic Effect (cm)
Time (days)

Figure 6

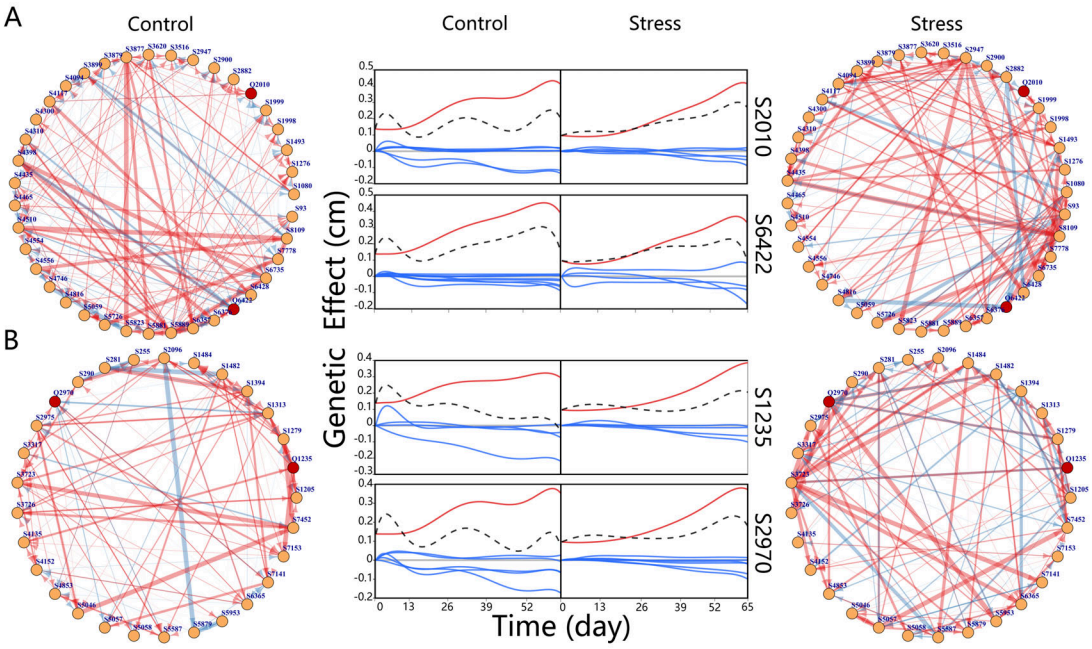
A
Control
Control
Stress
Stress
B
Genetic Effect (cm)
S2010
S6422
S1235
S2970
Time (day)